Reports

Mascons: Lunar Mass Concentrations

Abstract. *Lunar Orbiter tracking data have been processed to supply a qualitatively consistent gravimetric map of the lunar nearside. While a simplified model was employed, the results indicate that there are large mass concentrations under the lunar ringed maria. These mass concentrations may have important implications for the various theories regarding lunar history.*

The Lunar Orbiter missions have provided both high quality photographs of the moon, and supplementary scientific information concerning the gravitational field of the moon. Previous investigators have concluded that the moon was gravitationally rougher than anticipated in the sense that comparatively high degree terms in the spherical harmonic expansion would be required for effective representation of the gravity field (*1*). This roughness of the moon has been of interest to the Apollo Project because of the resulting perturbations on the trajectory of the Apollo orbiting spacecraft. For these reasons, a new analysis has been done with the use of the accurate tracking data received here by the NASA Deep Space Network operated by Jet Propulsion Laboratory.

We now report that this new processing (*2*) of the Lunar Orbiter data has produced unexpected results. A study of local accelerations on the spacecraft resulted in a gravipotential map (Fig. 1) of the lunar nearside which has revealed very large mass concentrations beneath the center of all five nearside ringed maria (Imbrium, Serenitatis, Crisium, Nectaris, and Humorum). In addition, they were observed in the area between Sinus Aestuum and Sinus Medii (presumably a newly discovered ancient ringed mare), and Mare Orientale. The Urey-Gilbert theory of lunar history (*3*) has predicted such large-scale high-density mass concentrations below these maria, which, for convenience, we shall call mascons.

The Deep Space Network tracks unmanned deep space probes launched by the United States. We use earth-based radio transmissions at 2300 Mhz in a coherent loop between the spacecraft and receiver. The doppler cycle count, which is the difference between the transmitted and the received signal, is continuously accumulated and sampled at regular 1-minute, 30-second or 10-second intervals. The high frequency noise on these data is between 0.1 and 1 mm/sec except at times of picture readout where the degradation factor is approximately 3. These data permit examination of the observed systematic effects which are in the neighborhood of 10 to 200 mm/sec (65 mm/sec = 1 hz).

Our sample of doppler data spans a 10-day period with 80 consecutive orbits of the Lunar Orbiter V spacecraft, during which it was continuously tracked. The spacecraft had the following orbital characteristics: semimajor axis, 2636 km; eccentricity, 0.27; inclination to the lunar equator, 85°; and orbital period, 3^h11^m. The closest approach to the lunar surface was 100 km at 2°N latitude.

The central 90-minute data span, centered on perilune, was taken from each individual orbit for the data processing. The combined coverage of the 80 orbits, south pole to north, east limb to west, was adequate to cover the lunar nearside hemisphere between ± 70° latitude and longitude.

Whereas the processing of the 9000 individual data points was a substantial undertaking, involving hand working of the punched cards, this was only a small fraction of the data available from five orbiters, in several mission phases, with distinct orbit characteristics.

These data were processed by least-squares fitting, in which the theoretical model (*4*) included a triaxial moon and gravitation perturbations due to the earth, the sun, Venus, Mars, Jupiter, and Saturn. It is necessary to limit the data arcs to 90 minutes in order to obtain the consistency required for the analysis. The method is described in reference (*2*), where the definite correlation between the residuals and variations in the lunar gravitational field is demonstrated.

The residuals from the raw doppler data, obtained after the best selenocentric position and velocity of the spacecraft have been estimated, become the data which are further processed. These data contain the local gravity effects, since the other variables such as station motion and the primary selenocentric orbit motion have been removed by the least-squares fit.

The next step in the reduction was to extract accelerations from the residuals. As shown in Fig. 2, they were fit with patched cubic polynomials (*5*) to smooth the data and to permit determination of an accurate derivative. Since the spacecraft altitude above the lunar surface is not constant, the raw accelerations represent the gravity effects at the height actually flown. What we really desired was a measure of the relative acceleration changes for a constant spacecraft altitude because such measurements would correlate with gravitational changes at or near the lunar surface. For that reason we normalized the accelerations so that the plotted values represent the acceleration a spacecraft would have experienced if it had been at an altitude of 100 km, under the assumption that the typical mascons were at a depth of 50 km below the surface, that is,

$$A_{\mathrm{norm}} = A_{\mathrm{comp}} \times (H + 50)^2/(150)^2$$

where A_{norm} is the normalized acceleration, A_{comp} is the computed acceleration, and H is the altitude in kilometers.

While this arbitrary choice was imposed upon us by our desire to make simplifying assumptions, we had some evidence as a basis for judgment. The analysis of distinct spacecraft (with different altitudes) flying over the same features had yielded 25 to 125 km for the depth of perturbing points below the surface. We therefore chose 50 km as an average depth expectation and used spacecraft accelerations normalized to the perilune distance of 100 km. Therefore the accelerations are based upon these assumptions.

The accelerations are of necessity measured along the spacecraft-earth direction. Since our method of data processing is a point-by-point scalar system, we are left with the unfortunate fact that a single data point cannot tell us from what direction the acceleration acted. What we see is the projection of the true acceleration on the spacecraft-earth vector. Only a modeled system fitting substantial quantities of continuous data can determine the nature of these geometrical effects.

Since the true direction of the forces is unknown, a simplifying assumption was made in order to tie the observed accelerations to the lunar surface for comparison with a map. Because the acceleration decreases with the distance squared, we assumed that the force was directly below the trajectory.

The decision to omit a correction for the projection on the spacecraft-earth vector, approximately a cosine function of the angular separation of the spacecraft from the lunar zero latitude and longitude point, resulted in increased uncertainty in the acceleration amplitudes near the limb. Such a correction seemed inadvisable because the true direction was unknown.

These constitute the simplifying assumptions that permitted rapid conversion of the raw residuals into gravimetric data. As already noted, the qualitative aspects of the new observations are rather well preserved at the expense of some of the quantitative information.

From the analysis so far we have ob-

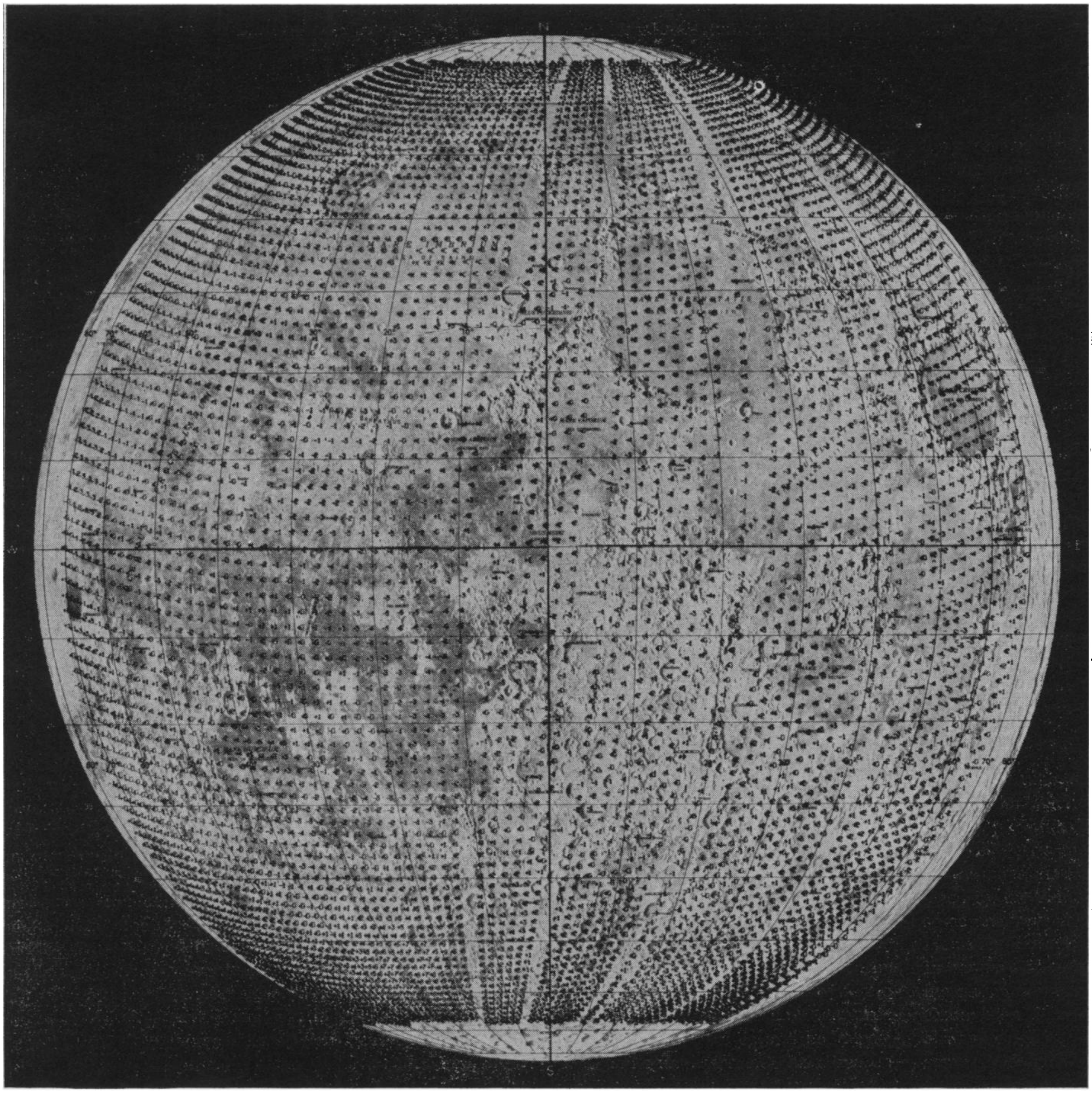

Fig. 1. Gravimetric and acceleration map of the lunar nearside. Ranges are indicated below.

Range *	Symbol	Range*	Symbol	Range*	Symbol
Beyond ±20.	±X	± 7.5 to ± 8.5	±8	± 2.5 to ± 3.5	±3
±15. to ±20.	±C	± 6.5 to ± 7.5	±7	± 1.5 to ± 2.5	±2
±11.5 to ±15.	±B	± 5.5 to ± 6.5	±6	± 0.5 to ± 1.5	±1
± 9.5 to ±11.5	±A	± 4.5 to ± 5.5	±5	0.0 to + 0.5	+0
± 8.5 to ± 9.5	±9	± 3.5 to ± 4.5	±4	− 0.5 to 0.0	−0

* Above × 0.1 = mm/sec^2; above × 10 = milligals; these scaling factors also apply to the cover.

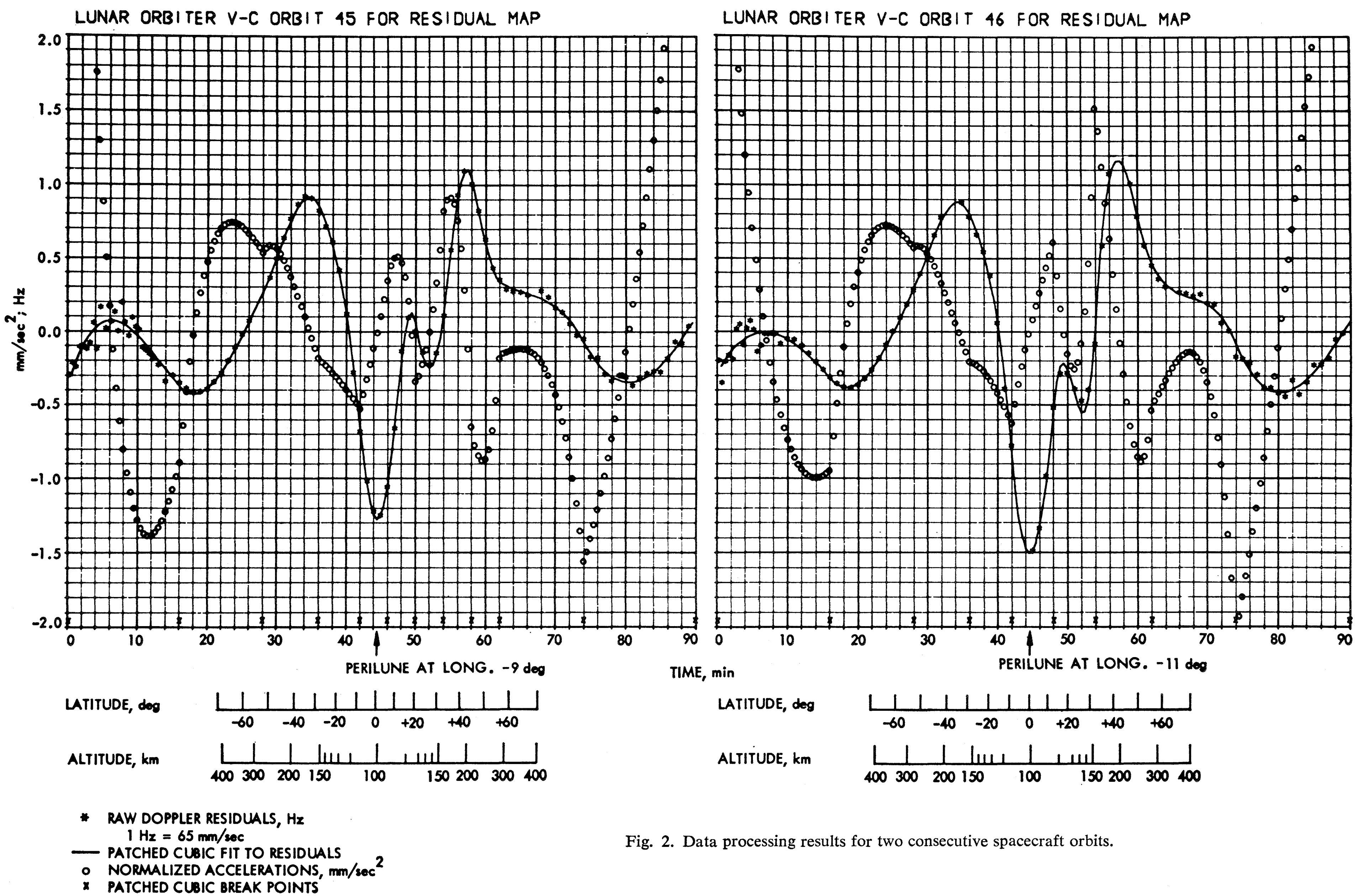

Fig. 2. Data processing results for two consecutive spacecraft orbits.

tained 74 sets (of the 80 orbits, 6 had insufficient data) of normalized accelerations (mm/sec^2) as shown in Fig. 1. While this approach was intended primarily to supply a priori information for a more quantitatively precise future analysis, the results proved to be very enlightening and of scientific importance. We emphasize that approximations were made, and those intending to analyze these data should use caution as dictated by the limitations on the method of data reduction.

A contour plot made from the data of Fig. 1 is shown on the cover. The large, distinct positive accelerations show clearly, along with a smaller number of distinct negative accelerations. Large positives lie in the centers of all five major ringed maria, (Imbrium, Serenitatis, Crisium, Humorum, and Nectaris). The large rate of change in the accelerations over these mascons reveals their relatively small physical extent (50 to 200 km). In fact, analysis of the detailed computer results indicates a nonspherical troughlike mass distribution (approximately 50 by 200 km, running generally east-west) in Imbrium and Serenitatis.

Apart from occasional short intervals of poor fit, the data are consistent. We have plotted the individual polar orbits (south to north) on Fig. 1. The consistency of the results can easily be seen by reading across the (Fig. 1) map, that is, from west to east, perpendicular to the individual polar orbits. The variations tend to be smooth and consistent across the adjacent orbit sets. Furthermore, computed comparisons between residual accelerations from an equatorial orbiter (Lunar Orbiter III) agree well with the plotted data. These results constitute the data consistency check and initial estimate of gravity variations which was sought from the simplified approach.

The more diffuse positive and negative variations shown on the plots near the limbs must be considered doubtful because of the normalizations introduced in the data processing. An orbit determination program, operating under a least-squares fitting, should minimize the sum of residuals squared and tend to compensate for large variations by "splitting the difference." Precisely how this effect has appeared in the results is difficult to determine with certainty, but we suspect that the large accelerations will give rise to diffuse, lower amplitude, opposite and compensating signatures in the processed data.

Table 1. Large positive mascon locations; P.E., probable error.

Ringed maria	Latitude (deg)		Longitude (deg)	
	Value	P.E.	Value	P.E.
Imbrium	32	1	−17	1
Serenitatis	25	1	19	1
Crisium	18	1	56	2
Nectaris	−15	1	33	1
Humorum	−23	1	−38	1
Orientale	−20	3	−95	3
Aestuum-Medii	6*	5	−6*	5

* Missing data and possible skewed fits make it impossible to ascertain whether there are one or two mascons in this location. More sophisticated processing and additional data from other orbiter missions will permit a determination.

The contour map shows two nearby mascons of intermediate magnitude between Sinus Aestuum and Sinus Medii. A crucial orbit is missing which might further clarify the situation, and it is not possible with these data to specify whether they are really distinct. However, this location certainly contains at least one definite mascon. It is consistent to assume that this represents an ancient feature similar to one of the modest ringed seas, obliterated by the debris from Serenitatis and Imbrium and only now revealed by the new data. There are other, lesser mascons which may or may not be significant. There may be correlations with the Russian magnetometer observations from their Luna probes if data over the specific indicated areas is analyzed. Their preliminary statement of results, however, does not indicate any unusual effects.

A side investigation of residuals not displayed in Fig. 2 was the examination of data in the area of Mare Orientale (−20° latitude, −95° longitude), a ringed mare discovered by Lunar Orbiter photography. If Orientale has the same characteristics of the other ringed maria, then high accelerations should occur directly above it. Since these largest accelerations would be normal to the probe-earth line at this longitude, one would expect essentially zero effect from the overflight orbit. However, from a family of orbits bracketing this time, we would expect those preceding the overflight to show a modest positive acceleration (at about −22° latitude), and those following to show a negative acceleration. The residuals from these several orbits were plotted and acceleration estimates were computed for latitude −22° with eight consecutive orbits (Table 2) resulting in precisely the effect predicted.

Table 2. Accelerations in the area of Orientale, 85° to 99°W longitude at a fixed 22°S latitude.

Orbit No.	Accelerations (mm/sec)^2
88	0.22
89	0.14
90	0.22
91	0.13
92	0.08
93	−0.17*
94	−0.17
95	−0.09
96	Occultation

* Taking geometry into account, and noting the zero-crossing in the table, permits determination of the Orientale mascon's longitude at −95°.

Examination of the detailed computer output permitted consistent estimates of the mascon locations. Results of these computations are presented in Table 1 with the estimated probable error.

Even though we have computed both masses and depths for the largest mascons, nevertheless our present quantitative data require further refinements. One may easily compute approximate masses from an assumed depth, such as 50 km. The Mare Imbrium mascon yields numbers on the order of 20×10^{-6} lunar masses. A spherical nickel-iron object about 100 km in diameter would be a rough equivalent. This type of calculation gives a qualitative estimate for the large size of these objects.

The presence of large mascons under every ringed maria, excepting Iridum, and their relative absence elsewhere, suggests a relation between the two phenomena which may be similar to that suggested by Urey and Gilbert (*3*). Among questions that arise are these: Does each of these mascons represent an asteroidal-sized body which caused its associated mare by impact? If not simply the original impactor itself, by what processes were they formed in the lunar interior? Is the presence of these objects consistent with a molten lunar interior?

Urey has proposed (*6*) that the Mare Imbrium collision object entered at Sinus Iridum as a low elevation impactor. Others have held that the two features are independent formations. Sinus Iridum is the smallest ringed mare and, Urey (*6*) and others (*7*) have pointed out, is a unique feature. It is larger than the other ringed and filled craters such at Ptolemaeus, and it has a similar appearance to the larger ringed maria discussed. If it is a separate impact mare, we expect that its physical properties would resemble the others, and hence contain a mascon for the same reasons.

Examination of the data reveals instead a sharply defined, negative acceleration. While this appears to support the Urey hypothesis, it is not necessarily inconsistent with other selelenological theories.

P. M. MULLER
W. L. SJOGREN

Jet Propulsion Laboratory, Pasadena, California

References and Notes

1. W. H. Michael, Jr., R. H. Tolson, J. P. Gapcynski, *Science* **153**, 1102 (1966); J. Lorell, in *Measure of the Moon*, Z. Kopal, Ed. (Gordon and Breach, New York, 1967); R. H. Tolson and J. P. Gapcynski, *Proc. Int. Space Sci. Symp. 8th* (COSPAR assembly, London, July 1967); J. Lorell and W. L. Sjogren, *Science* **159**, 625 (1968).
2. P. M. Muller and W. L. Sjogren, "Consistency of Lunar Orbiter residual with trajectory and local gravity effects," *Tech. Rep. 32-1072* (Jet Propulsion Laboratory, Pasadena, Calif.).
3. H. C. Urey, in *Vistas in Astronomy*, A. Beer, Ed. (Pergamon Press, London, 1956), vol. 2, p. 1676.
4. M. R. Warner and M. W. Nead, "SPODP—Single precision orbit determination program," *Tech. Mem. 33-204* (Jet Propulsion Laboratory, Pasadena, Calif., 1965).
5. T. M. Lang, "LEASTQ—A program for least-squares fitting segmented cubic polynomials having a continuous first derivative," *Space Programs Summary* (Jet Propulsion Laboratory, Pasadena, Calif., 1968).
6. H. C. Urey, in *Physics and Astronomy of the Moon*, Z. Kopal, Ed. (Academic Press, New York, 1962), pp. 484–486.
7. R. B. Baldwin, *The Face of the Moon* (Univ. of Chicago Press, Chicago, 1958), p. 200.
8. We thank R. W. Davies, W. L. Kaula, J. Lorell, P. Gottlieb, and D. W. Trask for many helpful contributions; D. K. Davies (and staff), R. Hanson, P. A. Laing, C. L. Lawson, and R. N. Wimberly for programming and computer assistance. This paper presents the results of one phase of research carried out at the Jet Propulsion Laboratory, California Institute of Technology, under NASA contract NAS 7-100.

1 August 1968

Potassium-Feldspar Phenocrysts in the Surface of Colomera, and Iron Meteorite

Abstract. *Silicate aggregates, including large single crystals of potassium feldspar as long as 11 centimeters and sodium feldspar, are embeded in the surface of the medium octahedrite Colomera. Silicate nodules in the interior appear to be much smaller (about 0.3 centimeter). Glass nodules are abundant both on the external surface and in the interior. These observations are evidence that some iron meteorites formed as segregations within a silicate matrix and did not originate in a metallic planetary core.*

The presence of silicates in iron meteorites has been well known for more than a century. Because of the obvious importance of the existence of the metallic iron, interest in the silicate fraction has been rather small until recently. The presence of a wide variety of silicates in iron meteorites (*1*) in much lower abundance than in pallasites and mesosiderites has permitted use of the Rb^{87}-Sr^{87} and K^{40}-Ar^{40} methods for the dating of these objects (*2*). Previous work in our laboratory on silicate inclusions from several iron meteorites showed very regular Rb^{87}-Sr^{87} and K^{40}-Ar^{40} ages of about 4.6×10^9 years. Silicate material taken from slices of Colomera yielded results that did not define an isochron. These anomalous results suggested that this meteorite merited further investigation.

Colomera, first recognized as an iron meteorite in 1934 (*3*), was found buried in a patio in the village of Colomera near Granada (Spain) in 1912. The original mass was reported as 134 kg; it measured roughly 50 by 40 by 16 cm. By courtesy of the Museo Nacional de Ciencias Naturales de Madrid, the main mass was shipped to our laboratory.

Preliminary observations showed that large silicate inclusions, partly obscured by rust, occur on the surface. In order to remove the rust, we cleaned the main mass by "sand blasting" with TiO_2 spherules. During this process it was discovered that the external surface contained at least four large silicate inclusions. One of these exhibited the characteristic reflectance of a single cleavage fragment; it was 11 cm long, 2.5 cm wide, and deeper than 1 cm. In the center of this inclusion were large green pyroxene aggregates ($\sim$ 1 cm). Several of the largest of these inclusions were found in depressions or "holes" in the surface. In addition to these large silicate masses, small ($\sim$ 0.3 cm) droplike masses were present on the external surface, resembling in size and form the silicate inclusions present in the interior and exposed on the cut surface. These small inclusions also occur in slices of Colomera. Some of the surface pockets are almost covered with silicates that suggest that they are relicts of a continuous filling of silicates. The silicates on the exterior can very easily be overlooked, since they often are rust colored.

The present mass of Colomera is 129.3 kg including all known pieces which are in the Spanish and U.S. National museums. Considering the thickness of the cuts made on this meteorite, and the loss of weight during removal of the rust, we can account for almost all the originally reported mass of 134 kg.

The surface of the meteorite shows clear evidence of subjection to some form of forging; hammer and chisel marks are obvious at several points. The extent to which the marks reflect its history before acquisition by the Spanish Museum is not obvious. Fractures in the meteorite and certain peculiar surfaces suggest that a fragment of iron was ripped away over a single area of about 100 cm^2. We cannot prove that the present surface is primary and was not significantly altered by ablation.

The mean density of the meteorite, determined on the main mass with a dynamometer in a Joly balance experiment, is 7.613 ± 0.048 g/cm^3. Estimating the densities of the metallic iron-nickel and silicate at 7.88 to 7.90 (*4*) and 3.3, respectively, and correcting for the presence of remnant rust, we obtain a range of 4.3 to 5.8 percent (by volume) of silicates in the whole meteorite. Clearly, large amounts of silicate inclusions are incompatible with the density data, the suggestion being that the abundance of large silicate masses on the exterior is not typical of the interior. This idea is supported by the observation that a large surface inclusion, exposed on the cut surface and in the adjacent slices, extends to a depth of only about 1 cm.

Several samples were taken from each of the large external-surface inclusions and from several of the small spheroidal inclusions exposed on both the external surface and the cut surface; they were studied optically, by x-ray diffraction and electron-microprobe techniques. Quantitative chemical analyses were obtained from the microprobe analyses using the procedures described by Bence and Albee (*5*). The average chemical analysis for each phase is reported in Table 1.

Macroscropic examination of the largest of the surface inclusions revealed two distinct phases: the large crystal (11 by 2.5 cm) already mentioned for which a cleavage face was observed, and aggregates or single crystals of green pyroxenes ($\sim$ 1 by 1 cm). Sam-